HHS Public Access

Author manuscript

Bone. Author manuscript; available in PMC 2017 October 01.

Published in final edited form as:

Bone. 2016 October ; 91: 81–91. doi:10.1016/j.bone.2016.07.007.

Combined treatment with a transforming growth factor beta inhibitor (1D11) and bortezomib improves bone architecture in a mouse model of myeloma-induced bone disease

Jeffry S. Nyman[a,b,c,d,*], **Alyssa R. Merkel**[a,c,e], **Sasidhar Uppuganti**[b], **Bijaya Nayak**[f], **Barbara Rowland**[a], **Alexander J. Makowski**[a,c,d], **Babatunde O. Oyajobi**[f,g], and **Julie A. Sterling**[a,c,d,e,h,*]

[a]Department of Veterans Affairs, Tennessee Valley Healthcare System, Nashville, TN 27212, USA

[b]Department of Orthopaedic Surgery & Rehabilitation, Vanderbilt University Medical Center, Nashville, TN 37232, USA

[c]Center for Bone Biology, Vanderbilt University Medical Center, Nashville, TN 37232, USA

[d]Department of Biomedical Engineering, Vanderbilt University, Nashville, TN 37232, USA

[e]Department of Medicine, Division of Clinical Pharmacology, Vanderbilt University Medical Center, Nashville, TN 37232, USA

[f]Department of Cellular and Structural Biology, University of Texas Health Science Center at San Antonio, San Antonio, TX 78229, USA

[g]The Cancer Therapy & Research Center, University of Texas Health Science Center at San Antonio, San Antonio, TX 78229, USA

[h]Department of Cancer Biology, Vanderbilt University, Nashville, TN 37232, USA

Abstract

Multiplemyeloma (MM) patients frequently develop tumor-induced bone destruction, yet no therapy completely eliminates the tumor or fully reverses bone loss. Transforming growth factor-β (TGF-β) activity often contributes to tumor-induced bone disease, and pre-clinical studies have indicated that TGF-β inhibition improves bone volume and reduces tumor growth in bone metastatic breast cancer. We hypothesized that inhibition of TGF-β signaling also reduces tumor growth, increases bone volume, and improves vertebral body strength in MM-bearing mice. We treated myeloma tumor-bearing (immunocompetent KaLwRij and immunocompromised Rag2 −/−) mice with a TGF-β inhibitory (1D11) or control (13C4) antibody, with or without the anti-myeloma drug bortezomib, for 4 weeks after inoculation of murine 5TGM1 MM cells. TGF-β inhibition increased trabecular bone volume, improved trabecular architecture, increased tissue mineral density of the trabeculae as assessed by ex vivo micro-computed tomography, and was associated with significantly greater vertebral body strength in biomechanical compression tests. Serum monoclonal paraprotein titers and spleen weights showed that 1D11 monotherapy did not

[*]Corresponding authors at: Vanderbilt Center for Bone Biology, 2215b Garland Avenue, Nashville, TN 37231, USA. jeffry.s.nyman@vanderbilt.edu (J.S. Nyman), julie.sterling@vanderbilt.edu (J.A. Sterling).

Appendix A. Supplementary data

Supplementary data to this article can be found online at http://dx.doi.org/10.1016/j.bone.2016.07.007.

reduce overall MM tumor burden. Combination therapy with 1D11 and bortezomib increased vertebral body strength, reduced tumor burden, and reduced cortical lesions in the femoral metaphysis, although it did not significantly improve cortical bone strength in three-point bending tests of the mid-shaft femur. Overall, our data provides rationale for evaluating inhibition of TGF-β signaling in combination with existing anti-myeloma agents as a potential therapeutic strategy to improve outcomes in patients with myeloma bone disease.

Keywords

Myeloma bone disease; Osteolysis; 1D11; Bortezomib; Bone architecture

1. Introduction

In patients with osteolytic cancer-induced bone disease, skeletal-related events (SREs) including pathologic fractures, spinal cord compression and hypercalcemia affect quality of life and survival [1,2]. Multiple myeloma (MM), the second most common adult hematologic malignancy, usually causes osteolytic bone disease in the axial and longitudinal skeleton. Bone loss due to excessive bone resorption weakens bone increasing the susceptibility to pathologic fractures and is responsible for the morbidity and mortality associated with the disease [3–5]. Bisphosphonates, the current standard-of-care for cancer-induced bone disease including MM, inhibit osteoclast function. However, even the most potent bisphosphonate, zoledronic acid, does not prevent fractures from eventually occurring in many patients, though it reduces the proportion of myeloma patients who experience SREs [6]. Resistance to fracture depends on trabecular architecture and overall quality of bone tissue. Therefore, continuing research to characterize molecular pathways that may lead to new bone formation and/or improve bone architecture and strength is necessary to facilitate development of novel bone anabolic agents as drugs to improve outcomes in MM.

Previous studies in MM and other bone metastatic diseases have shown that TGF-β contributes to tumor-induced bone disease [7–12]. Specifically, our group and others have demonstrated that TGF-β inhibition blocks tumor growth and osteoclast-mediated bone destruction. Importantly, TGF-β inhibition has been shown to improve bone quality beyond just inhibiting bone destruction [13]. That is, the material properties of mouse cortical bone (independent of bone structure) improve with a decrease in TGF-β signaling [13,14]. This suggests a potential benefit over using current standard-of-care osteoclast inhibiting approaches, such as bisphosphonates, that primarily affect trabecular architecture and volume. Therefore, inhibition of TGF-β signaling is an attractive therapeutic approach to treat MM-induced osteolytic bone disease.

Down-regulation of TGF-β signaling with the pan (binds to TGF-β 1, 2, and 3) anti-TGF-β neutralizing antibody, 1D11, improved bone parameters in various mouse models including a model of osteogenesis imperfecta [15] and a model of chronic kidney disease [16]. Inhibition of TGF-β with 1D11 also improved trabecular architecture as determined by micro-computed tomography (μCT) and cortical bone strength as determined by biomechanical analyses in normal non-tumor-bearing mice [14] as well as breast cancer

tumor-bearing mice [7]. In the latter, TGF-β inhibition also reduced tumor burden significantly [7]. While the role of TGF-β is relatively well characterized in breast tumors that metastasize to bone, its role in myeloma-induced bone disease remains less well defined [10].

Bortezomib, a United States Food and Drug Administration-approved proteasome inhibitor is a component of most combination regimens for first-line treatment of MM patients. Bortezomib not only exerts a robust anti-tumor effect in MM patients, it has been reported to also impact MM-induced bone disease by stimulating osteoblast differentiation in a bone morphogenetic protein (BMP)-dependent manner and by inhibiting dickkopf 1 (DKK1), a Wnt antagonist [17,18]. Other studies have shown that treatment with bortezomib may increase bone mineral density in MM tumor-bearing mice, in part, not only by stimulating osteoblastogenesis but also by inhibiting osteoclastogenesis [19]. However, there has been no detailed study investigating the effects of bortezomib on biomechanical parameters of bone quality in preclinical models of MM-induced osteolytic bone disease.

Since TGF-β signaling reportedly contributes to the progression of MM-induced bone diseases (reviewed in [5,10]), we hypothesized that inhibition of TGF-β signaling may reduce tumor growth, increase bone volume, and improve vertebral body strength in myeloma-bearing mice. The purpose of the present study was to investigate whether inhibition of TGF-β signaling in myeloma-bearing mice would reduce bone destruction and concomitantly promote bone strength. We used 1D11, a monoclonal antibody that neutralizes all 3 isoforms of TGF-β in rodents and has minimal effects on immune function in mice [20,21]. The monoclonal antibody 1D11 has been shown to inhibit metastases through effects on multiple cell types [22] and a humanized version of the antibody (GC1008, also known as *fresolimumab*) is currently being investigated in clinical trials as a therapeutic for several diseases including cancers [20,23]. Therefore, we treated MM tumor-bearing KaLwRij (immunocompetent) mice with 1D11 (or control 13C4 antibody) with or without bortezomib. Given the immune dysfunction commonly associated with MM patients [24], we also treated MM tumor-bearing Rag2 −/− (lacking B or T cells) mice with the same regimen. Tumor-burden was assessed by histology and by measuring monoclonal paraprotein titers in sera obtained from tumor-bearing mice *antemortem*. Bone quality was assessed post-mortem using a combination of μCT and biomechanical testing.

2. Materials and methods

2.1. Cell lines

The parental 5TGM1 MM cell line that was originally established from the Radl murine 5T33 myeloma model in the laboratory of Dr. Gregory Mundy, or a variant genetically engineered to stably express enhanced green fluorescent protein (GFP) (5TGM1-GFP cells) were used in this study. Both cell lines were obtained from the University of Texas Health Science Center at San Antonio (UTHSCSA) where they have been previously characterized [3,25]. For authentication, cells were routinely passaged through mice and monitored for signs of disease progression. This is one of the only pre-clinical myeloma models in which cells inoculated intravenously in naïve syngeneic host reproducibly induce osteolytic bone disease similar to what pertains in the human disease. The human myeloma cell line

RPMI8226 was obtained from the American Type Culture Collection (ATCC; Manassas, VA) and the human myeloma MM1.S cell line, originally obtained also from ATCC, was a gift from Dr. Joseph Agyin (UTHSCSA).

2.2. In vitro experiments

To evaluate TGF-β signaling in MM, 5TGM1-GFP cells were cultured in Roswell Park Memorial Institute (RPMI) medium supplemented with 10% fetal bovine serum (Atlas Biologicals, Fort Collins, CO) and 1% penicillin and streptomycin. Western blot for phosphorylated Smad 2/3 (pSmad 2/3) was performed using protein lysate from human or murine myeloma cells treated with TGF-β1 at 5 ng/mL with or without 1D11 or a control antibody (13C4) at 10 μg/mL. Protein was harvested 24 h after exogenous treatment with a Radio-immunoprecipitation assay (RIPA) buffer (Pierce, Life Technologies, Carlsbad, CA) supplemented with a protease and phosphatase inhibitor cocktail (Pierce). Protein concentration was determined by a bicinchoninic acid (BCA) protein assay (Pierce) according to instructions from the manufacturer. Protein (30 μg) was loaded onto a 10% sodium dodecyl sulfate polyacrylamide gel electrophoresis (SDS-PAGE) gel (Bio-Rad, Hercules, CA) and separated at 140 V. Proteins were transferred to a polyvinylidene difluoride (PVDF) membrane and blocked in blocking buffer (Leica Biosystems, Nussloch, Germany). Membranes were incubated overnight at 4 °C in an anti-pSmad 2/3 antibody (1:1000) (Cell Signaling Technology, Beverly, MA). A horseradish peroxidase goat anti-rabbit antibody (1:2000) (Cell Signaling) was used as the secondary antibody. Membranes were developed using a kit (Western Lightning Chemiluminescence Substrate kit, Perkin Elmer, Waltham, MA) and detected on a multispectral luminescence system (Bruker MS FX Pro Imaging System, Bruker Corp., Fremont, CA). Relative intensity was measured using ImageJ software (National Institutes of Health, Bethesda, MD).

To assess changes in tumor viability in response to TGF-β inhibition, a CellTiter 96® AQueous Non-Radioactive Cell Proliferation Assay (Promega Corporation, Madison, WI) was performed per manufacturer's instructions. Human or murine myeloma cells were plated in 96-well tissue culture plates and treated with 10 μg/mL 1D11 or 13C4 control. After adding solutions of 3-(4,5-dimethylthiazol-2-yl)-5-(3-carboxymethoxyphenyl)-2-(4-sulfophenyl)-2H-tetrazolium, inner salt (MTS) and phenazine methosulfate (PMS), cells were incubated at 37 °C in a CO2 incubator for 4 h and absorbance at 450 nm was recorded on a Synergy 2 multi-mode reader (BioTek, Winooski, VT). This protocol was performed at 0, 1, 3, and 5 days post 1D11-treatment.

2.3. In vivo study

5TGM1-GFP cells (5×10^5 cells in 100 μL phosphate-buffered saline [PBS]) were inoculated into 6- to 8-week-old Rag2 −/− mice (19 females and 17 males) (Taconic Biosciences, Germantown, NY, USA) or 6- to 8-week old naïve syngeneic C57BL/KaLwRijHsd mice (38 females) (Harlan, The Netherlands through Harlan, Indianapolis, IN) via the lateral tail vein. Starting on day 1 after tumor cell inoculation, the mice were randomized into groups (≥8 mice/group) for treatment as follows: (i) control isotype antibody (13C4); (ii) anti-TGF-β antibody (1D11); (iii) 13C4 and bortezomib; or (iv) 1D11 and bortezomib. Mice were treated for 4 weeks with antibody (10 mg/kg) with or without

bortezomib (0.5 mg/kg) by intraperitoneal injection 3 times per week. At 28 days post-tumor cell inoculation, when most mice had started to develop paraplegia, the experiment was terminated and the mice were sacrificed. Serum was collected by retro-orbital bleed at day 0, 3weeks after tumor cell inoculation, and just before sacrifice. All animal procedures adhered to a protocol approved by the local Institutional Animal Care and Use Committee at Vanderbilt University Medical Center.

2.4. Histomorphometry

Left hind limbs were excised at death; soft tissues were removed from the tibias and femurs; and femurs were fixed for 48 h in 10% neutral-buffered formalin. Fixed bones were decalcified in a 20% ethylenediaminetetraacetic acid (EDTA) solution for 48 h at room temperature and embedded in paraffin. Serial sections (thickness, 4 μm) were stained with either hematoxylin and eosin to define the region of interest (ROI) and the bone surface, tartrate resistant acid phosphatase (TRAP) to measure osteoclast number, or toluidine blue to measure osteoblast number. Sections were also used for immunohistochemistry to detect GFP expression in 5TGM1 MM cells as a surrogate marker for tumor volume.

The ROI was drawn around the endosteal surface of the metaphysis and below the growth plate to define the total area. After immunohistochemical staining using anti-GFP antibody (1:400 in 5% goat serum, 1 h at room temperature) (GeneTex, Irvine, CA), sections were counterstained lightly with hematoxylin and analyzed with an image analysis software (MetaMorph, Molecular Devices, Sunnyvale, CA). The number of GFP-positive cells was enumerated, and the percent of GFP-positive 5TGM1 myeloma cells per total area calculated. Mice with no detectable tumor by GFP-IHC were excluded from the analysis (3/36 for Rag2 −/− mice: 2-bortezomib, 1-1D11 + bortezomib and 8/38 for KaLwRij mice: 2-13C4, 2-1D11, 3-bortezomib, 1-1D11 + bortezomib). Osteoclasts and osteoblasts were assessed using Osteomeasure imaging software (OsteoMetrics, Decatur, GA). Stained sections were analyzed for osteoclasts by counting TRAP+ cells with 3 or more nuclei, and osteoblasts by counting blue/grey cuboidal cells found in clusters on the bone surface. Data presented as number of cells/bone surface.

2.5. Spleen weight analysis

Upon sacrifice, spleens were excised from the mice and immediately weighed. The average spleen weight was compared between treatment groups as an additional marker of overall tumor burden.

2.6. Enzyme-linked immunosorbent assay

Tumor burden was assessed using an in-house enzyme-linked immunosorbent assay as previously described [26]. Briefly, high-binding enzyme immunoassay/radioimmunoassay (EIA/RIA) plates (Corning Life Sciences, Corning, NY) were coated with an anti-IgG2bκ antibody (Fitzgerald Industries, Acton, MA) (2 μg/mL) overnight at 4 °C. Plates were washed with PBS with 0.5% Tween 20 (Sigma-Aldrich, St. Louis, MO) and blocked with 3% bovine serum albumin (BSA) in PBS. Serum samples were diluted 1:10,000 or 1:40,000 in 0.3% RIA-grade BSA in PBS and incubated for 1 h at room temperature. The detection antibody was added at 1:5000 dilution and incubated for 1 h at 37 °C. The *o*-

phenylenediamine dihydrochloride (OPD) reagent was used for detection, and samples were read at 450 nm on a plate reader (Synergy 2, BioTek). The concentration of IgG2bκ in each serum sample was calculated from a linear equation that was derived from a plot of known standards versus absorbance at 450 nm.

Collagen Type 1C-telopeptide (CTx) was measured from serum samples collected at sacrifice using a mouse CTX-1 competitive ELISA kit (Neo Scientific) following manufacturer's instructions. Briefly, samples were diluted 1:100. 100 μL samples and standards were added to the pre-coated microtiter plate and incubated for 1 h at room temperature. After thorough washing of the plate, 100 μL of HRP-conjugate was added to the plate and incubated for 1 h at 37 °C in a humidifying chamber, followed by washing and the addition of the substrate for 10 to 15 min. Samples were read at 450 nm on a plate reader (Synergy 2, BioTek). The concentration of CTX-1 in each serum sample was calculated from a linear equation that was derived from a plot of 1/known standards versus absorbance at 450 nm.

2.7. Micro-computed tomography (μCT)

The longitudinal axis of each excised right femur or each L6 vertebral body (VB) was aligned with the scanning axis of a high-resolution μCT scanner (μCT40, Scanco Medical, Brüttisellen, Switzerland). While immersed in phosphate buffered saline, the central portion of the femoral mid-shaft (1.2 mm), distal femoral metaphysis, and entire vertebral body were imaged at an isotropic voxel size of 12 μm (70 kVp/114 μA; 1000 projections per 360° rotation; integration time, 300 ms). To determine the structural characteristics of the femoral mid-shaft following standardized guidelines, contours were fit to the outer cortex using an auto-contouring script [27,28]. To determine architectural properties of trabecular bone [27], contours were fit within several voxels of the endosteum in the metaphysis or drawn by hand within the centrum of the vertebral bodies. The ROI for the metaphysis was 0.3 mm from the growth plate spanning 1.2 mm in the proximal direction, and the ROI for the vertebral body was the region between the two end plates. A consistent segmentation procedure was applied to all scans: global thresholds (and a Gaussian filter to suppress image noise) as 748.5 mg of hydroxyapatite (HA)/cm^3 (sigma = 0.8 with support of 2) for femoral cortex, as 414.5 mg HA/cm^3 (sigma = 0.2 with support of 1) for femoral metaphysis, and as 414.5 mg HA/cm^3 (sigma = 0.3 with support of 1) for vertebral body. Because the scanner was routinely calibrated to an HA phantom with a beam hardening correction from the manufacturer, we also obtained mean tissue mineral density (TMD) for both cortical (Ct) and trabecular (Tb) regions after segmentation.

To determine cortical porosity in the cortex of the femoral metaphysis, where multiple myeloma commonly induces osteolysis in tumor-bearing mice, we used a shell approach [29,30]. The outer contours around the periosteal edge of the metaphyseal cortex (avoiding the growth plate) were shrunk by 7 voxels to create 2 parallel contours within each cross section. These shell contours defined the ROI, and the scheme for the threshold (<415 mg HA/cm^3 with sigma = 0.5 and support of 2) inverted the image; therefore, the pores (not bone) became the segmented objects. Using the trabecular morphology script from the manufacturer, cortical porosity (Ct.Po), pore size (Ct.Po.Th), and pore number (Ct.Po.N)

data were obtained. Using this approach, we observed greater porosity in tumor- than in non-tumor-bearing mice (Supplemental Fig. 1).

2.8. Whole bone biomechanical testing

The mid-shaft of each hydrated femur was loaded to failure at 3 mm/min in three-point bending configuration with a span of 8 mm using a bench-top material testing system (DynaMight 8841, Instron, Canton, OH). Data for force versus displacement were recorded at 50 Hz from a 100 N load cell (Honeywell, Morristown, NJ, USA) and a linear variable displacement transducer. Whole bone stiffness was defined as the slope of the initial linear portion of the curve, and strength was the peak force recorded. Using the moment of inertia (I_{min}) of the femoral mid-shaft and the distance between the centroid and bone surface in the anteroposterior direction (c_{min}) from μCT, we estimated the modulus and strength from flexural equations [31].

Using the same material testing system, each hydrated vertebral body was subjected to axial compression at 3 mm/min. The supporting platen had a rough surface and moment relief to minimize slippage and off-axis loading, respectively. Vertebral body strength was defined as the peak force endured by the bone before failing.

2.9. Finite element analysis

To better understand how the drugs might increase vertebral body strength, μCT scans of the vertebral bodies were converted to finite element models (direct voxel-to-element conversion) using the Scanco FEA built-in solver (fe_solve3, v1.13, Scanco Medical AG, Brüttisellen, Switzerland). This elastic solver was used to determine the strain distribution for simulated high-friction, axial compression loading of each vertebral body to a peak level 1% apparent strain [32]. The elastic modulus was converted from TMD [33] (Poisson ratio was 0.3), in which elements were binned into 41 to 48 materials, depending on the TMD distribution of the scan. The predicted failure force was the point at which 2% of the bone tissue volume exceeded von Mises equivalent strain of 0.01.

2.10. Statistical analysis

Statistical analysis was performed with commercial software (GraphPad Prism, version 6.0a, GraphPad, La Jolla, CA). After determining whether each data set passed the Shapiro-Wilk normality test and that variance for each property was similar across the 4 groups (Bartlett's test), a one-way analysis of variance (passed tests) or Kruskal-Wallis test was used to determine whether significant differences existed among the experimental groups or time-points in the case of IgG2bκ titers. Holm-Sidak (parametric) or Dunn (non-parametric) multiple comparison tests were used to determine whether there was a difference i) between the control group (13C4) and each of the 3 treatment groups (13C4 vs 1D11, bortezomib, and 1D11 + bortezomib) or ii) between each treatment group (1D11 vs bortezomib, 1D11 vs 1D11 + bortezomib, and bortezomib vs 1D11 + bortezomib). Statistical significance was defined as $p \leq 0.05$.

3. Results

3.1. Signaling via the TGF-β receptor using 1D11 attenuates TGF-β-induced signaling in myeloma cells

To establish the importance of TGF-β signaling in MM, we determined the level of pSmad2/3, a primary mediator of canonical TGF-β signaling. As expected, pSmad was barely detectable in quiescent murine 5TGM1 myeloma cells as well as the human MM.1S, and RPMI8226 myeloma cells in the absence of exogenous TGF-β treatment (maintained under serum-free conditions overnight). However, phosphorylation of Smad was evident with the addition of exogenous TGF-β1 (Fig. 1A), indicating that the TGF-β signaling pathway is intact in all myeloma cells. Furthermore, pSmad was detected by immunohistochemistry in histologic sections of hind limbs from Rag2 −/− and KaLwRij mice inoculated with 5TGM1 cells (Fig. 1B) indicating that myeloma cells in the bone marrow microenvironment remain responsive to local TGF-β.

Treatment with the pan-TGF-β ligand inhibitory antibody 1D11 in vitro clearly attenuated pSmad in all three different cell lines (Fig. 1C), although the same antibody did not reduce the viability of any of the cell lines when treated at a dose of 10 μg/mL for up to 5 days as assessed by a MTS assay (Fig. 1D).

3.2. Treatment with 1D11 does not reduce tumor burden

Since TGF-β signaling pathway is intact in 5TGM1 cells, we hypothesized that TGF-β inhibition may reduce the development and/or progression of myeloma induced bone disease. To test these hypotheses, 5TGM1 tumor cells were inoculated into KaLwRij or Rag2 −/− mice and treated with control (13C4) antibody, 1D11, 13C4 and bortezomib, or 1D11 and bortezomib. At sacrifice (28 days), there was no reduction in spleen weight noted in either mouse strain treated with 1D11 (Fig. 2A). However, average spleen weight was lower in both mouse strains treated with a combination of bortezomib and 1D11 compared to tumor-bearing mice of either strain treated with control antibody or 1D11 antibody (Fig. 2A). Combined treatment with bortezomib and 1D11 decreased serum monoclonal paraprotein (IgG2bκ) titer, a marker of overall tumor burden, at 28 days (Fig. 2B). C-telopeptide of type I collagen (CTX), a serum marker for bone resorption, was reduced with 1D11 alone in KaLwRij mice only, while combined treatment with 1D11 and bortezomib decreased bone resorption in both strains relative to the 13C4 control (Fig. 2C). Treatment with 1D11 as a monotherapy had no effect on overall tumor burden in myeloma tumor-bearing mice (both mouse strains), despite significantly decreasing the levels of pSMAD 2/3 (Supplemental Fig. 2).

Consistent with this observation, histology showed that 1D11 did not reduce tumor area in bone (Fig. 3A, B). Although there was no change in tumor area in the 1D11-only group, Rag2 −/− mice that were treated with bortezomib and 1D11 had a significant reduction in tumor area in the bone with respect to control and anti-TGF-β treatment.

3.3. TGF-β inhibition improved bone parameters

Although 1D11 did not reduce tumor burden as hypothesized, we observed that combining 1D11 with bortezomib reduced porosity (osteolysis) in the outer metaphyseal cortex (Rag2 −/− mice, Fig. 4C; KaLwRij mice, Supplemental Table 1). This occurred primarily by a reduction in pore size (Fig. 4D) and not pore number (Fig. 4E). In relation to 13C4-treatment, bortezomib also reduced cortical lesions in Rag2 −/− mice (Fig. 4C).

With respect to 13C4 control, 1D11-treatment with and without bortezomib markedly increased trabecular bone volume fraction (BV/TV) in the femoral metaphysis (Tables 1 and 2) and the L6 vertebral body (VB) (Fig. 5A). The 1D11-treatment increased the trabecular number (Tb.N) in both mouse strains and increased trabecular thickness (Tb.Th) in the immunocompetent KaLwRij mice. The 1D11-treatment also improved trabecular architecture by increasing the connectivity density (Conn.D), number of plate-like trabeculae (structural model index [SMI], Tables 1 and 2), and trabecular tissue mineral density (Tb.TMD) of the VB only. Bortezomib alone had modest effects on trabecular bone, especially in the KaLwRij mice, but when combined with 1D11, there was an improvement in trabecular architecture as with 1D11 alone (Tables 1 and 2; Fig. 5B). In addition, vertebral body strength, as determined by compression testing (Fig. 5C) and finite element analysis (Fig. 5D) was higher for the 1D11-treated mice with or without bortezomib. The combination therapy did not improve VB strength beyond 1D11 mono-therapy, though it did result in higher VB strength than bortezomib treatment alone in the KaLwRij mice (Fig. 5C). The increase in strength occurred primarily from the increase in BV/TV, which accounted for 71.3% (KaLwRij mice) or 73.2% (Rag2 −/− mice) of the variance in peak force of the L6 VB. The predicted failure force accounted for 73.7% (Supplemental Fig. 3) or 69.9% of VB strength variance. Note that the predicted failure force includes the contribution of the cortical shell and TMD to compression strength in addition to trabecular architecture. Neither bortezomib nor combined treatment had an effect on the cortical bone of the diaphysis (Tables 1 and 2), except that stiffness was higher for 1D11 than 13C4 group in the Rag2 −/− mice (Table 2).

3.4. TGF-β inhibition increases osteoblast numbers in myeloma-bearing mice

In response to the observation of an increase in BV/TV, we examined histologic sections from these groups to determine whether these changes were caused by an increase in number of osteoblasts, reduction in number of osteoclasts, or a combination of changes in osteoblast and osteoclast number. 1D11-treatment, and combined treatment with 1D11 and bortezomib resulted in a significant increase ($p < 0.005$) in osteoblast number in Rag2 −/− and myeloma-bearing KaLwRij mice (Fig. 6A). Bortezomib treatment alone significantly increased osteoblast number in KaLwRij mice ($p < 0.05$). The number of osteoclasts in the hind limbs of tumor- bearing KaLwRij or Rag2 −/− mice decreased in response to bortezomib or combined treatment with 1D11 and bortezomib (Fig. 6B). 1D11-treatment alone had no effect on osteoclast number in comparison to 13C4-treatment.

4. Discussion

In the present study of MM-bearing mice, inhibition of TGF-β signaling by treatment with 1D11 improved trabecular microarchitecture, increased mineralization, and strengthened the lumbar vertebra when compared to control antibody therapy. Combining anti-MM therapy (bortezomib) with 1D11 had the same improvements in bone quality in addition to reducing tumor burden and cortical lesions. Translation of these bone effects to humans may result in prevention of vertebral body compression fractures and subsequently improve the quality of life of patients with MM.

The 5TGM1 murine model of myeloma is one of the best-characterized and closely recapitulates human bone disease [3,25,34]. The 5TGM1 model was originally developed, in part, to facilitate pre-clinical assessment of anti-tumor efficacy of novel agents in vivo and has been shown to be predictive of anti-tumor efficacy as demonstrated for bisphosphonate treatment, the current standard-of-care for cancer-induced bone diseases. While the use of a single myeloma model is clearly a limitation of the present study, other in vivo models do not effectively and/or reproducibly develop osteolytic bone disease as the 5TGM1 model. 5TGM1-GFP cells injected intravenously into syngeneic mice result in tumor growth within the bone marrow and spleen, an increase in serum monoclonal paraprotein, and characteristic osteolytic bone lesions. Furthermore, just like human myeloma cells (RPMI8226 and MM.1S), 5TGM1 cells also have an intact TGF-β signaling pathway and respond to TGF-β inhibition (Fig. 1). Taken together, these features of the 5TGM1 MM cells make this an ideal model to study effects of TGF-β inhibition on myeloma-induced bone disease.

Although the TGF-β signaling pathway is intact in the 5TGM1 cell line, monotherapy with 1D11 did not reduce tumor area (Fig. 3). Treatment with 1D11 did not however exacerbate tumor area in immunocompetent or immunocompromised mice. The absence of an effect on overall tumor burden is discordant with results observed for TGF-β inhibition by 1D11 in other tumor models, possibly because the medullary cavity is the primary site for MM unlike solid tumors such as breast and prostate that originate from other organ sites and are only metastatic to the bone marrow [15,31]. Primary bone marrow disease responds differently to TGF-β signaling than metastatic disease, and activation of signaling pathways may vary between progressive states [31]. However, why MM would respond differently to TGF-β is currently unclear.

The absence of reduction in tumor area in response to 1D11 was unexpected. The MM cells secrete TGF-β1, which stimulates bone marrow stromal cells to produce interleukin 6 (IL-6), a major growth factor for MM; inhibition of TGF-β1 blocks IL-6 production by bone marrow stromal cells [32]. Furthermore, a TGF-β receptor I kinase inhibitor, SD-208, decreased growth of MM cells in vitro, an effect reportedly mediated via adhesion of human MM cells to bone marrow stromal cells [33]. It is unknown why there was no reduction in tumor area in vivo in response to 1D11. It is possible that the dose of 1D11 used in this study, which was determined from previous studies, was not high enough to elicit anti-tumor effects in MM despite its efficacy in other models of tumor-induced bone disease. Further studies with different doses of 1D11 are needed to clarify the differential response in vivo to

TGF-β inhibition between MM and other bone metastatic cells. While TGF-β inhibition leads to a robust increase in bone volume in the MM model, concerns remain about possible off-target effects of inhibiting TGF-β signaling globally by a systemically-administered agent [35]. Nonetheless, TGF-β inhibition has been shown to be safe in clinical studies of fibrosis and cancer [20,21,23,36–38], suggesting its utility as a potential therapy for use in cancer -induced bone disease. It remains unclear how long term treatment with TGF-β may affect normal bone homeostasis and remodeling. Further preclinical studies of skeletal effects of inhibitors of TGF-β administered long-term are necessary to provide rationale for early stage clinical trials of this modality in combination with existing anti-MM agents in patients with MM-induced bone disease.

Several parameters varied between the 2 animal strains used in this study. Bortezomib alone significantly reduced spleen weight in the Rag2 −/− mice, but the combination of 1D11 and bortezomib was the only treatment that significantly reduced spleen weight in KaLwRij mice. There was also significantly less bone resorption, evidenced by lower cortical porosity, in the femoral metaphysis of bortezomib-treated Rag2 −/− mice when compared to the respective control mice (Fig. 4), whereas porosity was not significantly less for bortzomib-treated KaLwRij mice than for the respective control mice (Supplemental Table 1). Likewise, bortezomib was more effective in reducing tumor area in the metaphysis of Rag2 −/− mice than in the metaphysis of KaLwRij mice. While we are unsure of the cause of the discrepancy between these mouse strains, we hypothesize that the presence of the immune system in the KaLwRij mice may contribute, thus, emphasizing the importance of testing inhibitors in both immune competent and deficient models. Nonetheless and regardless of strain, combining bortezomib with 1D11 prevented osteolysis occurring in the cortex of the metaphysis. Although it is unknown which factors contributed to these differences, it is possible that immune system differences between the two mouse strains may be involved.

5. Conclusions

In summary, combined treatment with bortezomib and 1D11 reduced tumor area (an effect attributable to bortezomib alone) and improved bone quality (an unequivocal effect of 1D11). However, the present study suggests that monotherapy with TGF-β inhibitors is unlikely to be beneficial, contrary to the demonstration of bone anabolic effects of TGF-β inhibitors with other osteolysis-inducing tumor types [6]. Nevertheless, the present data provide rationale to explore approaches that inhibit TGF-β signaling (such as the humanized form of 1D11) in combination with a robust anti-myeloma agent (such as bortezomib) in the clinical management of MM patients to reduce bone destruction and pathological fractures and thereby improve overall quality of life.

Supplementary Material

Refer to Web version on PubMed Central for supplementary material.

Acknowledgments

The authors thank Dr. Patrick Finn and Genzyme (Sanofi) for the gift of 1D11 and 13C4 that made these studies possible. We (JAS/JSN/BOO) also thank our mentor, Dr. Gregory Mundy, whose ideas and VA Merit Award helped initiate these studies and kept them funded even after his untimely death.

This work was supported by grants from the Veterans Administration (VA): I01BX001957 (JAS), I01BX001018 (JSN), I01BX000327 (JAS/JSN) and the NIH: R01CA163499 (JAS).

References

1. Coleman R, et al. Bone health in cancer patients: ESMO Clinical Practice Guidelines. Ann Oncol. 2014; 25(Suppl. 3):iii124–iii137. [PubMed: 24782453]
2. Saad F, et al. Pathologic fractures correlate with reduced survival in patients with malignant bone disease. Cancer. 2007; 110(8):1860–1867. [PubMed: 17763372]
3. Garrett IR, et al. A murine model of human myeloma bone disease. Bone. 1997; 20(6):515–520. [PubMed: 9177864]
4. Terpos E, et al. Management of bone disease in multiple myeloma. Expert. Rev. Hematol. 2014; 7(1):113–125. [PubMed: 24433088]
5. Silbermann R, Roodman GD. Myeloma bone disease: Pathophysiology and management. J. Bone Oncol. 2013; 2(2):59–69. [PubMed: 26909272]
6. Rosen LS, et al. Long-term efficacy and safety of zoledronic acid compared with pamidronate disodium in the treatment of skeletal complications in patients with advanced multiple myeloma or breast carcinoma: a randomized, double-blind, multicenter, comparative trial. Cancer. 2003; 98(8): 1735–1744. [PubMed: 14534891]
7. Biswas S, et al. Anti-transforming growth factor β antibody treatment rescues bone loss and prevents breast cancer metastasis to bone. PLoS One. 2011; 6(11):e27090. [PubMed: 22096521]
8. Javelaud D, et al. Efficient TGF-beta/SMAD signaling in human melanoma cells associated with high c-SKI/SnoN expression. Mol. Cancer. 2011; 10(1):2. [PubMed: 21211030]
9. Johnson RW, et al. TGF-beta promotion of Gli2-induced expression of parathyroid hormone-related protein, an important osteolytic factor in bone metastasis, is independent of canonical hedgehog signaling. Cancer Res. 2011; 71(3):822–831. [PubMed: 21189326]
10. Matsumoto T, Abe M. TGF-beta-related mechanisms of bone destruction in multiple myeloma. Bone. 2011; 48(1):129–134. [PubMed: 20570621]
11. Mohammad KS, et al. TGF-beta-RI kinase inhibitor SD-208 reduces the development and progression of melanoma bone metastases. Cancer Res. 2011; 71(1):175–184. [PubMed: 21084275]
12. Yin JJ, et al. TGF-beta signaling blockade inhibits PTHrP secretion by breast cancer cells and bone metastases development. J. Clin. Invest. 1999; 103(2):197–206. [PubMed: 9916131]
13. Balooch G, et al. TGF-beta regulates the mechanical properties and composition of bone matrix. Proc. Natl. Acad. Sci. U. S. A. 2005; 102(52):18813–18818. [PubMed: 16354837]
14. Edwards JR, et al. Inhibition of TGF-beta signaling by 1D11 antibody treatment increases bone mass and quality in vivo. J. Bone Miner. Res. 2010; 25(11):2419–2426. [PubMed: 20499365]
15. Grafe I, et al. Excessive transforming growth factor-beta signaling is a common mechanism in osteogenesis imperfecta. Nat. Med. 2014; 20(6):670–675. [PubMed: 24793237]
16. Liu S, et al. Role of TGF-beta in a mouse model of high turnover renal osteodystrophy. J. Bone Miner. Res. 2014; 29(5):1141–1157. [PubMed: 24166835]
17. Page JM, et al. Matrix rigidity regulates the transition of tumor cells to a bone-destructive phenotype through integrin beta3 and TGF-beta receptor type II. Biomaterials. 2015; 64:33–44. [PubMed: 26115412]
18. Richardson PG, Hideshima T, Anderson KC. Bortezomib (PS-341): A novel, first-in-class proteasome inhibitor for the treatment of multiple myeloma and other cancers. Cancer Control. 2003; 10(5):361–369. [PubMed: 14581890]

19. Pennisi A, et al. The proteasome inhibitor, bortezomib suppresses primary myeloma and stimulates bone formation in myelomatous and nonmyelomatous bones in vivo. Am. J. Hematol. 2009; 84(1): 6–14. [PubMed: 18980173]
20. Lonning S, Mannick J, McPherson JM. Antibody targeting of TGF-beta in cancer patients. Curr. Pharm. Biotechnol. 2011; 12(12):2176–2189. [PubMed: 21619535]
21. Ruzek MC, et al. Minimal effects on immune parameters following chronic anti- TGF-beta monoclonal antibody administration to normal mice. Immunopharmacol. Immunotoxicol. 2003; 25(2):235–257. [PubMed: 12784916]
22. Nam JS, et al. An anti-transforming growth factor beta antibody suppresses metastasis via cooperative effects on multiple cell compartments. Cancer Res. 2008; 68(10):3835–3843. [PubMed: 18483268]
23. Stevenson JP, et al. Immunological effects of the TGFbeta-blocking antibody GC1008 in malignant pleural mesothelioma patients. Oncoimmunology. 2013; 2(8):e26218. [PubMed: 24179709]
24. Binsfeld M, et al. Cellular immunotherapy in multiple myeloma: lessons from preclinical models. Biochim. Biophys. Acta. 2014; 1846(2):392–404. [PubMed: 25109893]
25. Oyajobi BO, et al. Detection of myeloma in skeleton ofmice by whole-body optical fluorescence imaging. Mol. Cancer Ther. 2007; 6(6):1701–1708. [PubMed: 17541032]
26. Oyajobi BO, et al. Dual effects of macrophage inflammatory protein-1alpha on osteolysis and tumor burden in the murine 5TGM1 model of myeloma bone disease. Blood. 2003; 102(1):311–319. [PubMed: 12649140]
27. Bouxsein ML, et al. Guidelines for assessment of bone microstructure in rodents using micro-computed tomography. J. Bone Miner. Res. 2010; 25(7):1468–1486. [PubMed: 20533309]
28. Buie HR, et al. Automatic segmentation of cortical and trabecular compartments based on a dual threshold technique for in vivo micro-CT bone analysis. Bone. 2007; 41(4):505–515. [PubMed: 17693147]
29. Fowler JA, et al. Host-derived adiponectin is tumor-suppressive and a novel therapeutic target for multiple myeloma and the associated bone disease. Blood. 2011; 118(22):5872–5882. [PubMed: 21908434]
30. Nyman JS, et al. Quantitative measures of femoral fracture repair in rats derived by micro-computed tomography. J. Biomech. 2009; 42(7):891–897. [PubMed: 19281987]
31. Turner RT, et al. Acute exposure to high dose gamma-radiation results in transient activation of bone lining cells. Bone. 2013; 57(1):164–173. [PubMed: 23954507]
32. Nyman JS, et al. Predicting mouse vertebra strength with micro-computed tomography-derived finite element analysis. Bonekey Rep. 2015; 4:664. [PubMed: 25908967]
33. Easley SK, et al. Contribution of the intra-specimen variations in tissue mineralization to PTH- and raloxifene-induced changes in stiffness of rat vertebrae. Bone. 2010; 46(4):1162–1169. [PubMed: 20034599]
34. Lawson MA, et al. Osteoclasts control reactivation of dormantmyeloma cells by remodelling the endosteal niche. Nat. Commun. 2015; 6:8983. [PubMed: 26632274]
35. Bierie B, Moses HL. Gain or loss of TGFbeta signaling in mammary carcinoma cells can promote metastasis. Cell Cycle. 2009; 8(20):3319–3327. [PubMed: 19806012]
36. Hau P, et al. Inhibition of TGF-beta2 with AP 12009 in recurrent malignant gliomas: from preclinical to phase I/II studies. Oligonucleotides. 2007; 17(2):201–212. [PubMed: 17638524]
37. Morris JC, et al. Phase I study of GC1008 (fresolimumab): a human anti-transforming growth factor-beta (TGFbeta) monoclonal antibody in patients with advanced malignant melanoma or renal cell carcinoma. PLoS One. 2014; 9(3):e90353. [PubMed: 24618589]
38. Trachtman H, et al. A phase 1, single-dose study of fresolimumab, an anti-TGF-beta antibody, in treatment-resistant primary focal segmental glomerulosclerosis. Kidney Int. 2011; 79(11):1236–1243. [PubMed: 21368745]

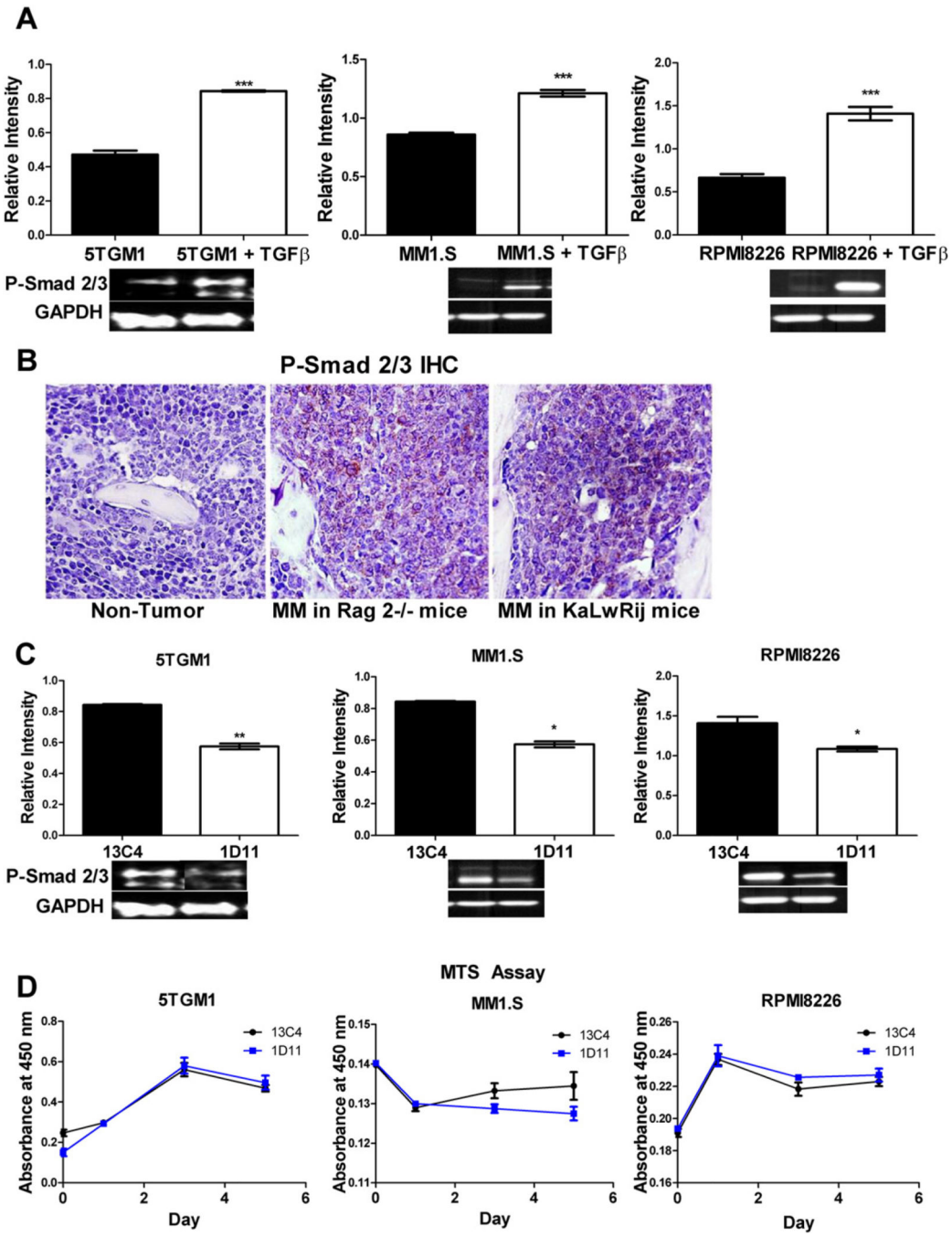

Fig. 1.

In vitro assay of transforming growth factor β (TGF-β) activity in multiple myeloma cells. Expression of pSmad 2/3 in 5TGM1, MM1.S, and RPMI8226 MM cells by (A) Western blot and (B) immunohistochemistry in bone sections from 5TGM1 tumor-bearing mice, indicating intact constitutive TGF-β signaling pathway in 5TGM1 cells in vitro and in vivo. (C) Exposure of 5TGM1 MM1.S, and RPMI8226 cells to 1D11 attenuated phosphorylation of Smad 2/3 in response to exogenous TGF-β. (D) Exposure to the antibody did not reduce viability of any cell line as evidenced by an MTS assay. $*p < 0.05$ $***p < 0.001$

Abbreviations: GADPH, glyceraldehyde 3-phosphate dehydrogenase; IHC, immunohistochemistry; MM, multiple myeloma; pSmad, phosphorylated Smad 2/3.

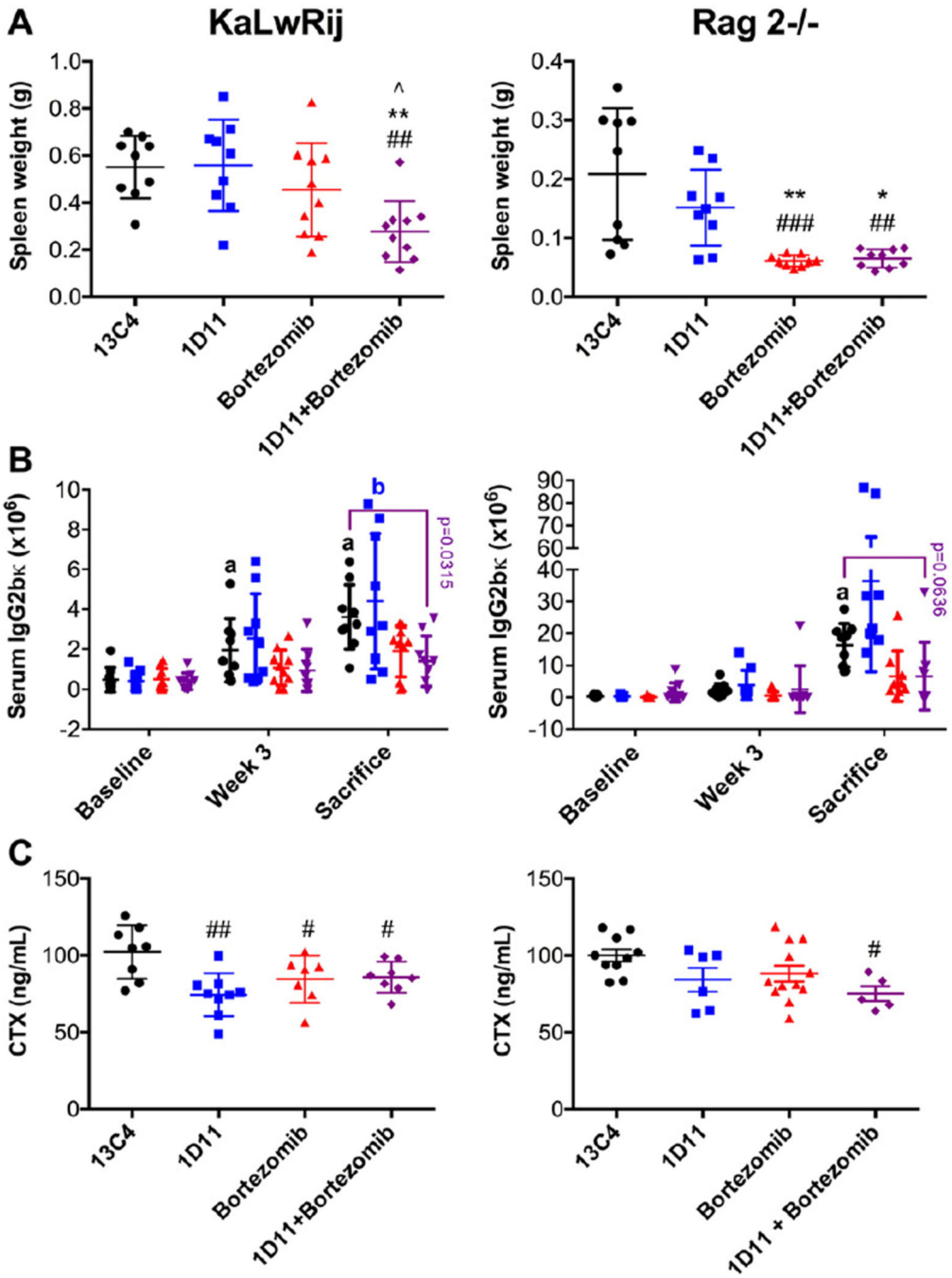

Fig. 2.

Effect of treatment with 1D11 and/or bortezomib on overall multiple myeloma tumor burden. Combined treatment with 1D11 and bortezomib reduced overall tumor burden in both mouse strains, as shown by a reduction in (A) spleen weight (B) serum paraprotein (IgG2bκ) titer and (C) serum CTX concentration. Normal mouse spleen weight is ≤0.1 g. Treatment with 1D11alone did not affect the temporal increase in MM tumor burden. Comparisons vs 13C4: #$p < 0.05$, ##$p < 0.01$, and ###$p < 0.001$; Comparisons vs 1D11: *p

< 0.05 and **p < 0.01; Comparison vs Bortezomib: ^p < 0.05; and Comparisons vs baseline: ap < 0.05 within 13C4 and bp < 0.05 with 1D11.

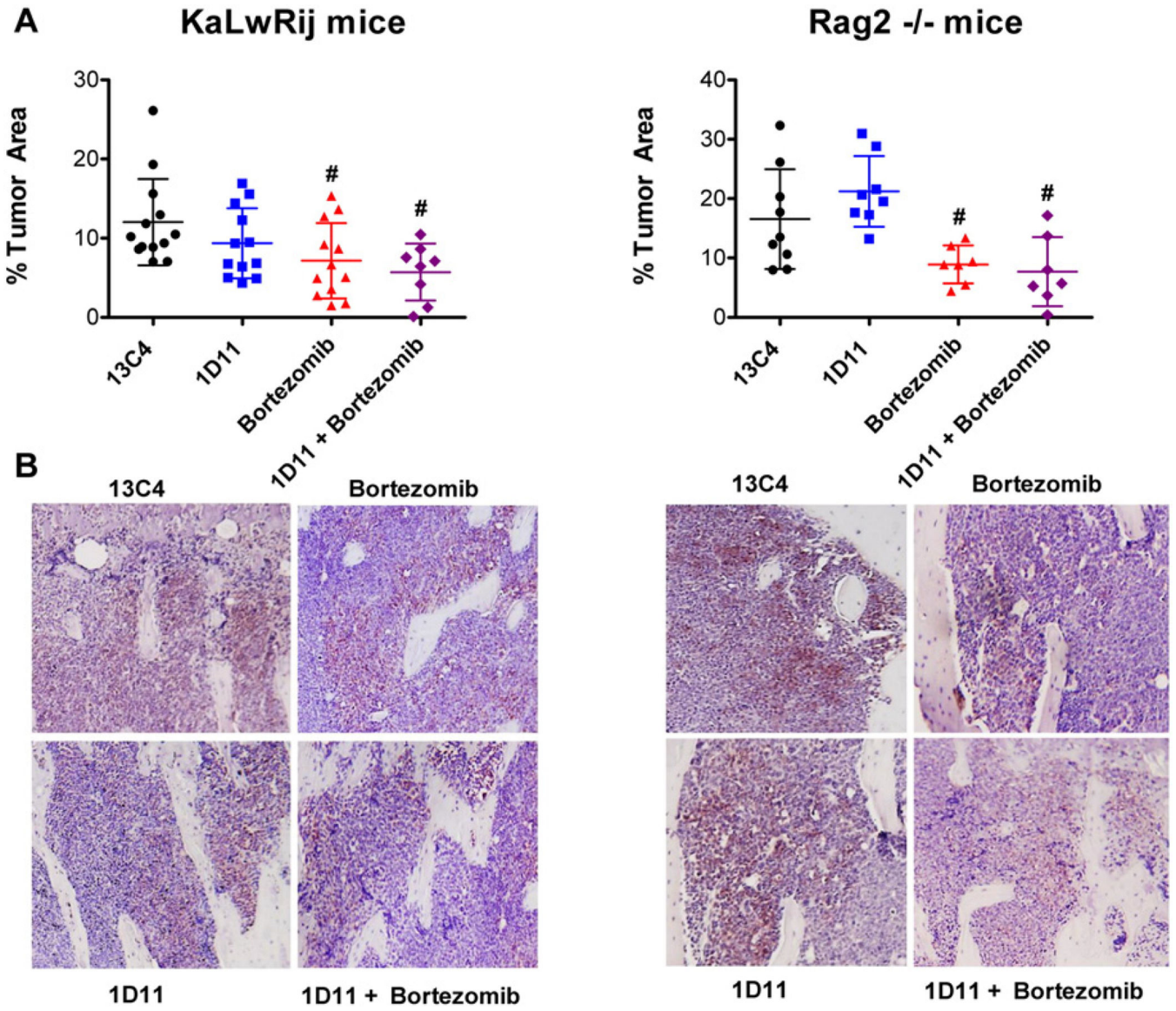

Fig. 3.

Effect of treatment with 1D11 and/or bortezomib on multiple myeloma tumor area. (A) Quantification of (B) immunohistochemistry images for anti-GFP (targeting 5TGM1-GFP tumor cells) showed decreased tumor area in hind limbs of KaLwRij mice and Rag2 −/− mice when treated with the combination of bortezomib and 1D11. Bortezomib treatment alone decreased tumor area in Rag2 −/− mice. Comparisons vs 13C4: #$p < 0.05$ and Comparisons vs 1D11: *$p < 0.05$ and **$p < 0.01$.

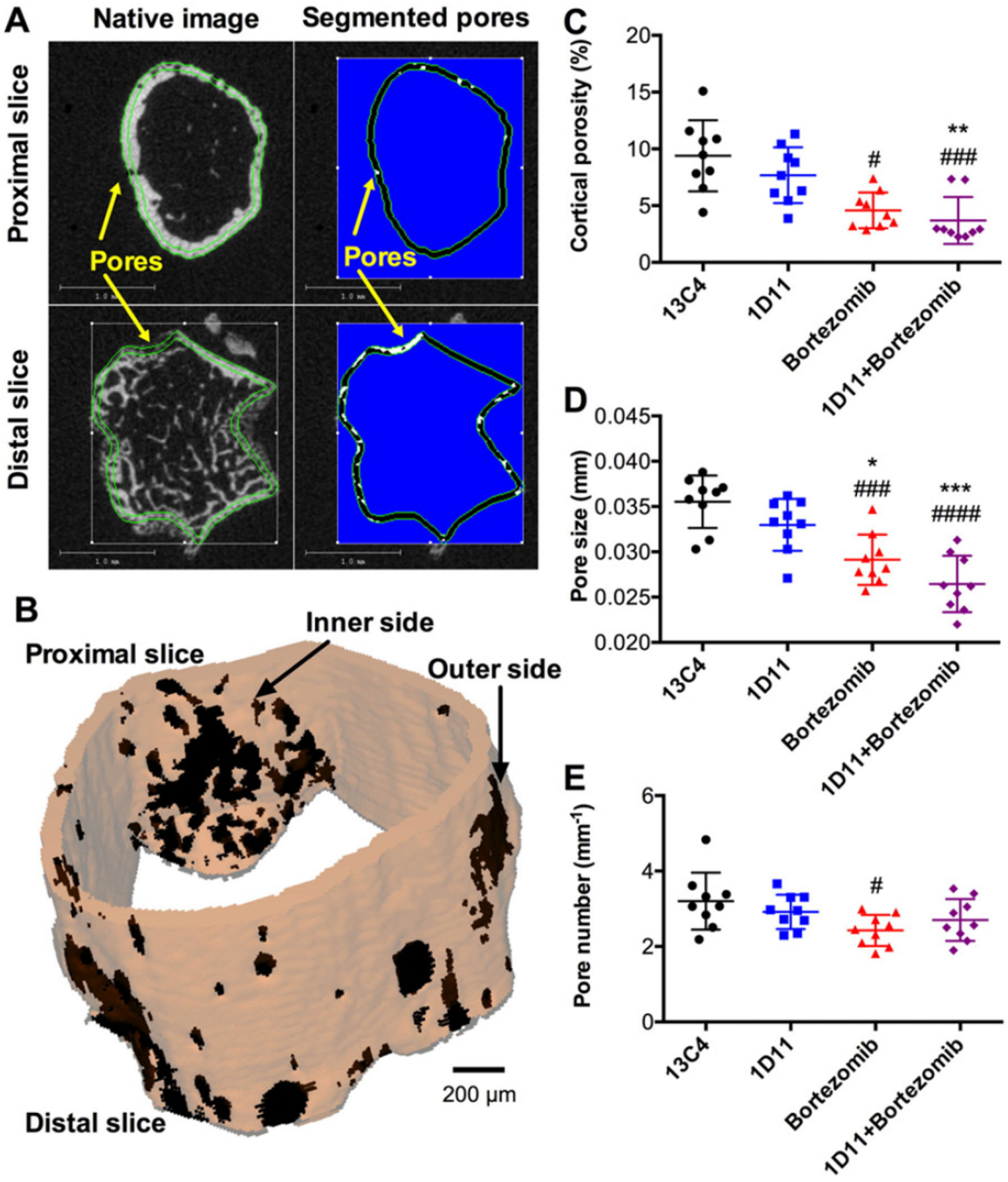

Fig. 4.

Effect of treatment with 1D11 and/or bortezomib on cortical porosity in metaphysis of long bones from MM tumor-bearing mice. Using the shell technique separated by 7 voxels, lesions were quantified within the cortex of the femur metaphysis (A). A representative rendering shows regions of possible osteolysis as pores depicted in dark brown (B). As shown here for the Rag2 −/− mice, bortezomib alone as well as the combination of 1D11 and bortezomib reduced (C) cortical porosity, (D) pore size, and (E) pore number. Similar results were obtained with the KaLwRij mice. Comparisons vs 13C4: #$p < 0.05$, ###$p <$

0.001, and ####$p < 0.0001$ and Comparisons vs 1D11: *$p < 0.05$ and ***$p < 0.001$. (For interpretation of the reference to color in this figure legend, the reader is referred to the web version of this article.)

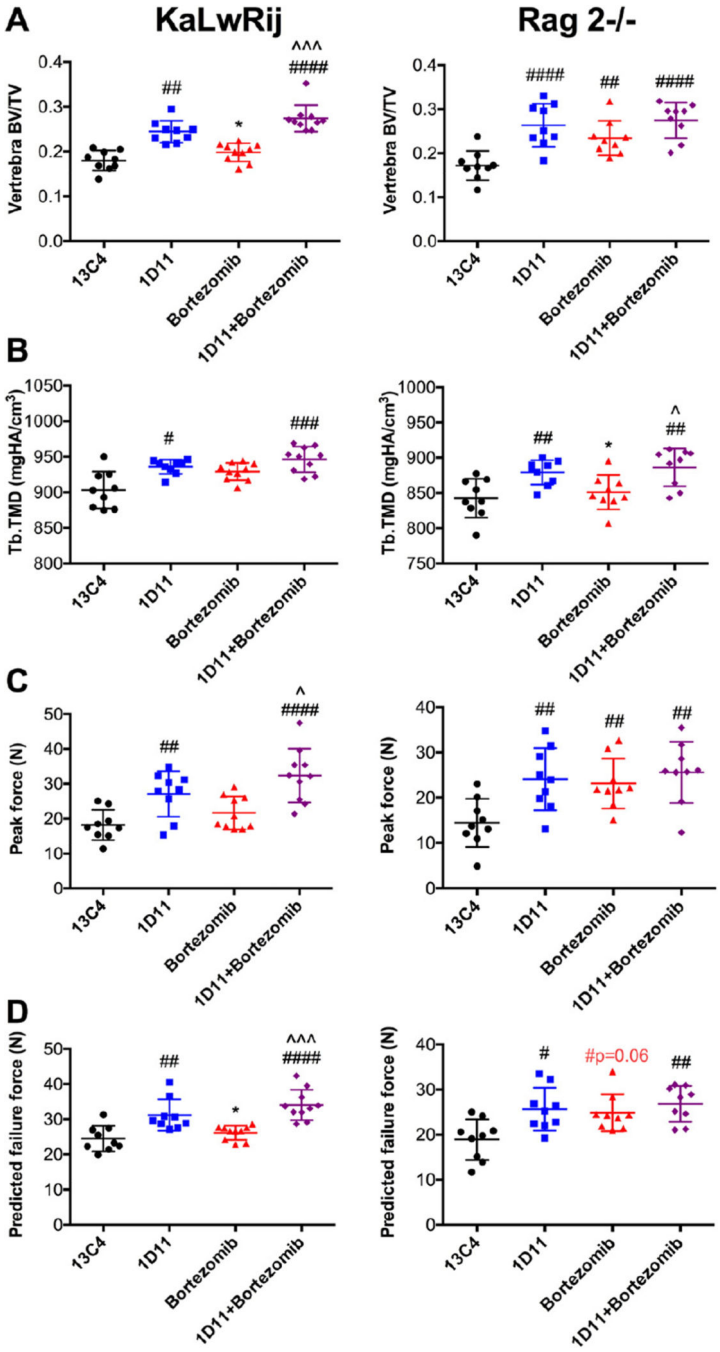

Fig. 5.

Effect of treatment with 1D11 and/or bortezomib on parameters of bone strength and quality in L6 vertebrae from KaLwRij and Rag2 −/− tumor-bearing mice. Treatment with 1D11, with and without bortezomib, increased trabecular bone volume fraction (A), tissue mineral density (B), experimentally-determined vertebral body (VB) strength (C), and predicted VB strength (D) in both mouse strains engrafted with multiple myeloma cells. Comparisons vs 13C4: #$p < 0.05$, ##$p < 0.01$, ###$p < 0.001$, and ####$p < 0.0001$; Comparisons vs 1D11:*$p < 0.05$; and Comparison vs bortezomib: ^$p < 0.05$ and ^^^$p < 0.001$.

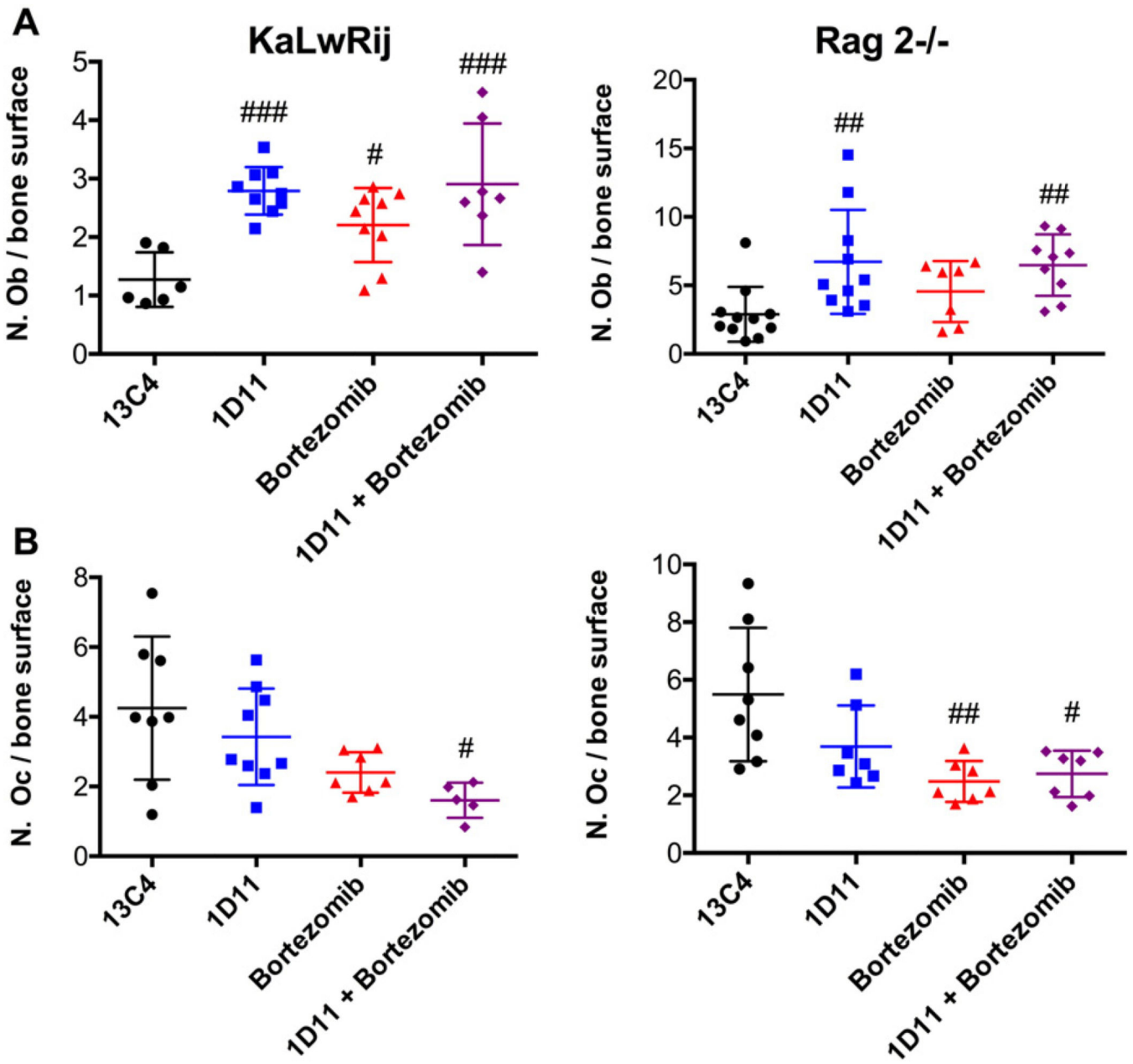

Fig. 6.

Effect of treatment on osteoblast and osteoclast number. There was a significant increase in (A) osteoblast counts in KaLwRij mice and Rag2 −/− tumor-bearing mice in response to 1D11 monotherapy or combined treatment with 1D11 and bortezomib. (B) Osteoclast counts for either tumor-bearing KaLwRij or Rag2 −/− mice were decreased in response to bortezomib treatment or combined treatment with 1D11 and bortezomib. Comparison vs 13C4: #$p < 0.05$, ##$p < 0.01$, ###$p < 0.001$, and ####$p < 0.0001$.

Table 1

Effect of treatment on trabecular bone architecture and cortical bone strength for the femur of tumor-bearing KaLwRij mice.

Property	13C4	1D11	Bortezomib	Bortezomib + 1D11
Metaphysis				
Trabecular bone volume fraction (BV/TV)	0.048 ± 0.011	**0.118 ± 0.023**[a,b]	0.058 ± 0.015	**0.140 ± 0.049**[a,b]
Trabecular number (Tb.N) (mm^{-1})	3.81 ± 0.40	**4.90 ± 0.41**[a,b]	3.84 ± 0.47	**4.98 ± 0.52**[a,b]
Trabecular thickness (Tb.Th) (mm)	0.037 ± 0.003	**0.041 ± 0.002**[a]	0.039 ± 0.002	**0.043 ± 0.004**[a,b]
Trabecular spacing (Tb.Sp) (mm)	0.265 ± 0.028	**0.203 ± 0.020**[a,b]	0.264 ± 0.034	**0.200 ± 0.022**[a,b]
Connectivity density (Conn.D) (mm^{-3})	43 ± 21	**178 ± 31**[a,b]	51 ± 31	**189 ± 51**[a,b]
Structural model index (SMI)	3.37 ± 0.23	**2.42 ± 0.22**[a,b]	3.18 ± 0.26	**2.24 ± 0.51**[a,b]
Trabecular tissue mineral density (Tb.TMD) (mg HA/cm3)	950 ± 16	954 ± 14	951 ± 8	964 ± 10
Diaphysis				
Length (mm)	13.1 ± 0.2	13.1 ± 0.3	13.2 ± 0.5	13.2 ± 0.3
Moment of inertia (Imin) (mm4)	0.084 ± 0.010	0.090 ± 0.013	0.087 ± 0.007	0.085 ± 0.012
Cortical tissue mineral density (Ct.TMD) (mg HA/cm3)	1245 ± 20	1241 ± 16	1240 ± 15	1247 ± 13
Stiffness (N/mm)	71.3 ± 18.6	74.1 ± 16.6	66.8 ± 11.8	80.2 ± 11.8
Peak force (N)	13.4 ± 1.2	13.5 ± 1.3	13.4 ± 1.0	13.7 ± 1.1
Modulus (GPa)	9.0 ± 2.0	8.8 ± 1.6	8.2 ± 1.2	10.1 ± 1.1
Bending strength (MPa)	194.9 ± 13.5	189.8 ± 13.9	193.3 ± 10.8	202.4 ± 14.3

mg HA = mg hydroxyapatite.

[a] Bold indicates the statistically significant difference compared to 13C4 (control); $p < 0.05$ vs 13C4.

[b] Bold indicates the statistically significant difference compared to Bortezomib; $p < 0.05$ vs Bortezomib.

Table 2

Effect of treatment on trabecular bone architecture and cortical bone strength for the femur of tumor-bearing Rag2−/− mice.

Property	13C4	1D11	Bortezomib	Bortezomib + 1D11
Metaphysis				
Trabecular bone volume fraction (BV/TV)	0.057 ± 0.020	**0.116 ± 0.008**[a]	0.078 ± 0.019	**0.194 ± 0.027**[a,b]
Trabecular number (Tb.N) (mm-1)	3.39 ± 0.38	**4.65 ± 0.15**[a,b]	3.70 ± 0.54	**4.95 ± 0.26**[a,b]
Trabecular thickness (Tb.Th) (mm)	0.041 ± 0.006	0.040 ± 0.002	0.041 ± 0.002	**0.048 ± 0.003**[a,b,c]
Trabecular spacing (Tb.Sp) (mm)	0.299 ± 0.035	**0.212 ± 0.007**[a,b]	0.276 ± 0.045	**0.196 ± 0.012**[a,b]
Connectivity density (Conn.D) (mm^{-3})	55 ± 23	**174 ± 27**[a,b]	**96 ± 37**[a]	**223 ± 32**[a,b,c]
Structural model index (SMI)	3.11 ± 0.25	**2.29 ± 0.14**[a,b]	**2.71 ± 0.24**[a]	**1.36 ± 0.34**[a,b,c]
Trabecular tissue mineral density (Tb.TMD) (mgHA/cm3)	906 ± 27	920 ± 18	909 ± 23	911 ± 21
Diaphysis				
Length (mm)	13.6 ± 0.4	13.3 ± 0.3	13.3 ± 0.3	13.5 ± 0.4
Moment of inertia (Imin) (mm^4)	0.074 ± 0.007	0.077 ± 0.008	0.069 ± 0.009	0.076 ± 0.016
Cortical tissue mineral density (Ct.TMD) (mg HA/cm^3)	1200 ± 16	1220 ± 20	1212 ± 21	1198 ± 12
Stiffness (N/mm)	61.2 ± 9.7	**74.3 ± 11.8**[a]	59.6 ± 7.6	69.8 ± 9.3
Peak force (N)	12.3 ± 1.0	13.0 ± 1.2	11.8 ± 0.9	12.4 ± 1.2
Modulus (GPa)	8.8 ± 0.8	**10.3 ± 1.6**[a]	9.2 ± 1.2	9.9 ± 1.3
Bending strength (MPa)	190 ± 10	197 ± 16	198 ± 22	193 ± 16

[a] Bold indicates the statistically significant difference compared to 13C4 (control). $p < 0.05$ vs 13C4.

[b] Bold indicates the statistically significant difference compared to Bortezomib; $p < 0.05$ vs Bortezomib.

[c] Bold indicates the statistically significant difference compared to 1D11; $p < 0.05$ vs 1D11.